Research Square

Preprints are preliminary reports that have not undergone peer review.
They should not be considered conclusive, used to inform clinical practice,
or referenced by the media as validated information.

Tuning Cellulose Nanocrystals from Hemp Agro-Waste: Effect of Reaction Time on Surface Properties, Wettability, and Biocompatibility

Jesse A. Heacock
Colorado State University
Mahboube Piryaee
Colorado State University
Morgan Davis
Colorado State University
Yan Li
yan.li@colostate.edu

Colorado State University

Research Article

Keywords: Cellulose Nanocrystals (CNCs), Ammonium Persulfate (APS) Oxidation, Hemp Agro-waste, Surface Functionalization, Physicochemical Properties, Biomedical Coatings

Posted Date: October 23rd, 2026

DOI: https://doi.org/10.21203/rs.3.rs-9509082/v1

License: This work is licensed under a Creative Commons Attribution 4.0 International License.
Read Full License

Additional Declarations: No competing interests reported.

Abstract

This study investigates how ammonium persulfate (APS) oxidation reaction time influences the physicochemical and biological properties of cellulose nanocrystals (CNCs) derived from hemp agro-waste. CNCs prepared at reaction times from 8 to 48 h were systematically evaluated for size, surface chemistry, colloidal stability, mechanical strengths, wettability, and cytotoxicity. Atomic force microscopy (AFM) revealed that CNC length decreased significantly with reaction time, from 467 ± 277 nm (8h) to 159 ± 67 nm (48h). Fourier transform infrared spectroscopy (FTIR) confirmed progressive removal of lignin and hemicellulose, along with the incorporation of sodium carboxyl groups. Despite these structural changes, AFM force-distance spectroscopy showed a consistent Young's modulus of approximately 73.00 GPa, independent of reaction times. Titanium (Ti) substrates coated with CNCs exhibited enhanced hydrophilicity compared to bare Ti, with wettability strongly dependent on CNC extraction time. Cytotoxicity assays with human adipose-derived stem cells confirmed non-toxic behavior across all reaction times. Collectively, these results demonstrate that APS oxidation time provides a tunable and sustainable parameter for tailoring CNC surface and interfacial properties without compromising mechanical integrity or cytocompatibility, supporting their potential use in biomedical coating and other high-value biomedical applications.

Introduction

Cellulose is the most abundant renewable polymer on Earth, produced at an estimated rate of over 10^{10} tons annually, and is a major component of agricultural and forestry residues (Delepierre *et al.* 2021; Mali and Sherje 2022). Structurally, cellulose is a linear homopolymer of glucose residues connected by β-1,4-glycosidic bonds, with alternating amorphous and crystalline regions. Selective removal of amorphous domains yields cellulose nanocrystals (CNCs); rod-like nanoparticles typically 5–50 nm in diameter and 100–500 nm in length. CNCs combine high aspect ratios, stiffness, hydrophilicity, biocompatibility, biodegradability, and a chemically modifiable surface, making them attractive for diverse applications ranging from sustainable packaging and coatings to tissue engineering scaffolds, drug delivery systems, gene therapy vectors, and medical devices (Patil *et al.* 2022; Punia Bangar *et al.* 2023).

Numerous strategies have been developed for CNC extraction, including mechanical, chemical, and enzymatic methods (Man *et al.* 2011; Benhamou *et al.* 2014; Novo *et al.* 2015; Kang *et al.* 2018). Among these, acid hydrolysis is the most widely used, but it generates large amounts of acidic effluent and introduces sulfate ester groups that may compromise thermal stability and biocompatibility, limiting biomedical and green applications. As an alternative, ammonium persulfate (APS) oxidation has emerged as a biofriendly, one-step method that both isolates CNCs and introduces carboxyl groups, enhancing colloidal stability and surface functionality (Leung *et al.* 2011; Lam *et al.* 2013; Castro-Guerrero and Gray 2014; Jiang *et al.* 2017; Oun and Rhim 2018; Bashar *et al.* 2019; Filipova *et al.* 2020; Wang *et al.* 2020; Liu et al. 2020; Culsum *et al.* 2021; Khanjanzadeh and Park 2021; Marwanto *et al.* 2021; Haunreiter et al. 2022; Madani *et al.* 2022). APS oxidation involves a swelling stage at room temperature, followed by heat-induced decomposition of peroxydisulfate into sulfate free radicals, which remove

amorphous cellulose while leaving the crystalline domain intact. Subsequent surface oxidation generates carboxylic acid groups, producing carbonylated CNCs with improved functionalities for further modifications (Lam *et al.* 2013; Haunreiter et al. 2022).

APS oxidation has demonstrated versatility across a wide range of raw materials, including recycled fiberboard (Khanjanzadeh and Park 2021), jute fiber (Bashar *et al.* 2019), industrial denim waste (Culsum *et al.* 2021), popular residues (Jiang *et al.* 2023), balsa and kapok fibers (Marwanto *et al.* 2021), rice straw (Oun and Rhim 2018), and hemp hurds (Wang *et al.* 2020). These studies highlight APS as a scalable and sustainable method for valorizing low-value biomass into functional nanomaterials. However, the physicochemical and biological properties of CNCs are highly sensitive to extraction conditions, including precursor type, temperature, pH, and reaction time. CNC properties such as particle size, morphology, crystallinity, thermal stability, surface charge, and cytotoxicity have been reported to vary with processing parameters (Bashar *et al.* 2019; Culsum *et al.* 2021; Marwanto *et al.* 2021; Haunreiter et al. 2022). In particular, reaction time during APS oxidation has been identified as an important but underexplored factor that may control CNC yield, functional group incorporation, and interfacial behavior.

Tuning CNC properties is especially important for biomedical surface coatings. One particularly promising application is the modification of titanium (Ti) implant surfaces. Ti is widely used for orthopedic and dental implant materials due to its corrosion resistance, mechanical strength, and intrinsic biocompatibility (Vilaça *et al.* 2021; Asad and Sana 2023; Jiang *et al.* 2023). However, long-term clinical success depends on surface modification strategies that improve osseointegration, reduce immune responses, and promote cell adhesion and proliferation (Liu et al. 2020). Current approaches to Ti modification include altering micro- and nano-scale topography, adjusting wettability, and introducing cytocompatible or antimicrobial coatings (Liu et al. 2020; Akshaya *et al.* 2022; Asad and Sana 2023; Im *et al.* 2023; Thu *et al.* 2023; Piryaee et al. 2025). CNCs, with their tunable surface chemistry and inherent hydrophilicity, represent a promising natural nanomaterial for such applications. Therefore, controlling APS oxidation time could enable precise tailoring of CNC surface properties to optimize interfacial behaviors with Ti and improve biomedical performance.

Despite the increasing adoption of APS oxidation for CNC extraction, the influence of APS reaction time on CNC structure and properties and the resulting implications for surface and interfacial performance remain insufficiently understood. In this study, CNCs were extracted from hemp hurds using APS oxidation with reaction times ranging from 8 to 48 hours to systematically examine this processing parameter. We hypothesized that APS oxidation reaction time governs the extent of cellulose oxidation and fibril cleavage, resulting in predictable changes in CNC dimensions and surface chemistry that enable tunable interfacial wettability on Ti substrates, while preserving intrinsic mechanical stiffness and cytocompatibility. CNC yield, size, morphology, and surface wettability were evaluated, along with their effects on Ti substrates wettability and cytotoxicity toward human adipose-derived stem cells. The results confirm that CNC size and surface chemistry are strongly dependent on APS oxidation time, leading to tunable effects on titanium surface wettability, while mechanical stiffness (~ 73 GPa) and

cytocompatibility remained unchanged. These results demonstrate, for the first time, that APS reaction time provides a simple and sustainable lever to tailor CNC interfacial properties without compromising their intrinsic mechanical or biological performance. This work establishes a sustainable pathway for producing functional nanomaterials from agricultural residues for biomedical and other high-value applications.

Materials and experiments

Materials

Raw hemp (*Cannabis Sativa* L.) hurds, obtained after fiber removal by retting and mechanical separation, were provided by a local hemp farm in Fort Collins, CO, USA. The hurds were milled into fine powder using a mechanical blender (Cincred MC-BL618). Ammonium persulfate (APS, ≥ 98%) was purchased from Sigma Aldrich, and sodium hydroxide (NaOH, 99.4%) from Fisher Scientific. All reagents were used as received. Titanium (Ti) foils (0.05 mm thickness) were purchased from EdgeTech Industries LLC (Parkland, FL). Human adipose-derived stem cells (hASCs) were obtained from Sanguine Laboratory (San Diego, CA) and cultured according to the supplier's instructions.

CNC extraction by APS oxidation

Wang et al. (2020) demonstrated a modified APS oxidation method, which was used to extract CNCs in this study. Briefly, hemp hurd powder (2 g) was dispersed in 100 ml of 2 M APS solution and stirred at 150 rpm for 3 hours to allow swelling. The suspension was then heated to 60°C while stirring at 350 rpm to initiate the oxidation process. Reaction time of 8, 12, 16, 20, 24, 36, and 48 hours were employed, yielding samples denoted as 8-CNC, 12-CNC, 16-CNC, 20-CNC, 24-CNC, 36-CNC, and 48-CNC. After reaction, products were collected by centrifugation at 6000 rpm for 15 minutes (VWR Clinical 200), washed repeatedly with deionized water until pH ~ 4, neutralized to pH 7 with 1 M NaOH, and washed again. Final suspensions were stored in the wet state or lyophilized for further analysis.

Yield determination

CNC suspensions were frozen at -80°C for 24 hours and dried using a freeze dryer (Labconco FreeZone 4.5–50°C) for 24 hours, or until samples were completely dry. Yield (%) was determined as:

$$\%yield = \frac{dry\,CNC\,weight\ (g)}{HAW\,powder \times \%cellulose\,content\ (g)} \times 100$$

1

Based on prior reports, the cellulose content of hemp hurds was assumed to be 40% (Momeni *et al.* 2021).

Fourier transform infrared spectroscopy (FTIR)

The chemical structure of CNCs was analyzed by ATR-FTIR (Cary 630, Agilent Technology) over 650–4000 cm^{-1} with a resolution of 2 cm^{-1} and 32 scans. Lyophilized CNC powders were used for the analysis.

Dynamic light scattering (DLS) and zeta potential

Particle size and zeta charge were measured using a Zetasizer Nano ZS (Malvern Instruments). CNCs were dispersed in deionized water (0.0004% w/v, pH 7) at room temperature. Hydrodynamic size was determined in disposable cuvettes, and zeta potential by M3-PALS in capillary cells. Six replicates were measured per sample.

Atomic force microscopy (AFM) morphological analysis

CNC morphology was assessed by AFM imaging (XE-70, Park System). Mica substrates were pretreated with 0.01% poly-L-lysine, rinsed, and dried. CNC suspensions (0.04% w/v) were deposited, spin-coated, and dried in a desiccator. Topographical images were collected in contact mode using CONTSCR probes (tip radius ~ 10 nm, spring constant ~ 0.2 N/m), and CNC dimensions were analyzed using ImageJ software.

AFM – force distance spectroscopy (FDS)

In contrast to AFM imaging used for morphological analysis, mechanical characteristics of CNCs were evaluated using AFM force–distance spectroscopy (FDS). Mechanical characteristics for 8-CNC, 24-CNC, and 48-CNC samples were selectively evaluated using AFM force-distance spectroscopy (XE-70, Park Systems) with NC-LC probes (tip radius ~ 20 nm, spring constant ~ 100 N/m). Fifty individual CNCs per sample were tested to determine Young's modulus and adhesion energy. Young's modulus and adhesion energy were extracted from force–distance curves using established contact mechanics models.

Wettability of CNC-coated titanium

Ti foils were cut into 2 × 2 cm pieces, cleaned by sequential sonication in acetone, isopropanol, and deionized water, and dried in a desiccator. CNC suspension (4% w/v) was dropped onto the Ti surface and dried under ambient conditions. Static water contact angles were measured with a goniometer (Attension Theta Flex, Biolin Scientific) using a sessile drop method.

Cytotoxicity

CNC suspension (1 mg/mL) was prepared in α-MEM growth medium (HyClone™), sterilized by filtration (0.22 µm), and incubated for 12 hours before use. hASCs were seeded in 48-well plates and cultured for 24h before treatment. CNC-containing media were added, and cells were incubated for 24 hours. Cytotoxicity was assessed by LDH assay (Quantichrom, BioAssay Systems) according to the manufacturer's protocol. Absorbance was measured at 490 and 680 nm using a microplate reader (Fluostar Omega, BMG LABTECH) (Madruga *et al.* 2020). Five replicates were tested per condition.

Statistical analysis

All experiments were performed in triplicate unless otherwise noted. Results are expressed as mean ± standard deviation. Statistical analysis was performed using two-way ANOVA with Tukey's multiple comparison test (R Studio), with significance set at $p < 0.05$.

Results and discussion

CNC dispersion and colloidal stability

The dispersion and colloidal stability of CNCs were evaluated as a function of APS oxidation reaction time. For medical applications, it is important to link extraction parameters to predictable changes in particle stability. CNCs were extracted from hemp hurds by APS-assisted swelling, followed by oxidation for varying reaction times (Wang *et al.* 2020). The oxidation introduces surface carboxyl groups, imparting a negative net charge. Zeta potential analysis confirmed that all CNCs had charges below − 25 mV (Fig. 1i); the threshold generally considered to ensure colloidal stability in aqueous suspensions. Reported values ranged from − 33.1 to -47.2 mV, consistent with previous studies of APS-derived CNCs, which typically fall between − 30 and − 40 mV (Bashar *et al.* 2019; Wang *et al.* 2020).

To further assess long-term stability, 4% (w/v) CNC suspensions were stored for up to three months. 36-CNC and 48-CNC were the most homogeneous and transparent, while 8-CNC and 12-CNC remained opaque and eventually formed visible aggregates (Fig. 1a-g). This trend of decreasing opacity with increasing reaction time agrees with earlier reports (Wang *et al.* 2020). Interestingly, despite 8-CNC showing the lowest zeta potential (-47 mV), its aqueous suspension aggregated after three months, suggesting that other parameters beyond surface charge, such as particle size and residual impurities, might influence long-term stability. Dynamic light scattering (DLS) confirmed systematic changes in particle size with reaction time (Fig. 1h). Longer reaction times are correlated with smaller particle sizes, as summarized in Table 1. For example, 8-CNC and 12-CNC displayed larger hydrodynamic radii compared to later samples, which remained stable and more homogeneous. These results indicate that while zeta potential confirms short-term stability, opacity and DLS measurements reveal that CNCs produced at longer reaction times (≥ 16 h) are more uniform, colloidally stable, and resistant to aggregation over time.

Size, morphology, and yield

The effect of APS reaction time on CNC yield and dimensions was further examined. Lyophilized CNCs collected at different reaction times showed clear visual differences: as reaction time increased, the powders shifted in color from tan to bright white (Fig. 2a-g), consistent with the progressive removal of lignin and hemicellulose. At the same time, overall yield decreased substantially with longer oxidation, from 709 mg (88.6%) at 8 h to only 22 mg (2.8%) at 48 h (Table 1). Intermediate yields included 51.5% at 12 h, 36.8% at 16 h, 23.5% at 20 h, 33.8% at 24 h, and 25% at 36 h. These values align with previous studies, such as 64 – 54% yield from jute fibers for 6–24 h reactions *(Bashar* et al. *2019)*. These results confirm that extended reaction times improve purification, but significantly reduce recovery efficiency.

AFM topographical images obtained by contact-mode imaging further revealed systematic size and dispersion changes (Fig. 3). All CNCs displayed the typical needle-like morphology across all samples (Fig. 3a-g), consistent with previous CNC studies (Bashar *et al.* 2019; Culsum *et al.* 2021; Marwanto *et al.* 2021; Haunreiter et al. 2022). Early samples (8-CNC and 12-CNC) appeared larger and more aggregated, often overlapping. By contrast, CNCs obtained after longer oxidation times were smaller, better separated, and more uniform. This trend is highlighted by the scale bars: 1000 nm for 8-CNC and 12-CNC versus 500 nm for later samples. Quantitative analysis confirmed these visual **Fig. 3** AFM images (first and second rows), length distribution (h), and width distribution (i) of 8-CNC (a), 12-CNC (b), 16-CNC (c), 20-CNC (d), 24-CNC (e), 36-CNC (f), and 48-CNC (g)

differences. 8-CNC had the largest mean length (467 ± 277 nm) and width (31.9 ± 9.3 nm), while 48-CNCs were the smallest, at 159 ± 63 nm in length and 19.9 ± 3.4 nm in width. Aspect ratios decreased from 14.9 at 8h to 8.1 at 48h, with intermediate values showing some overlap. Importantly, size distributions narrowed with increasing reaction time (Fig. 3h-i), indicating more uniform particle populations. Overall, these results demonstrate that the APS oxidation time strongly influences CNC yield, size, and uniformity. Longer reaction times improve homogeneity and reduce particle dimensions, but at the cost of lower recovery, highlighting a trade-off between efficiency and material quality.

Table 1
Physicochemical properties of CNCs extracted at different APS oxidation times

Reaction Time (hours)	DLS hydrodynamic radius (nm)	Zeta Potential (mV)	CNC Dry Weight (mg)	CNC yield (%)	CNC Length (nm)	CNC Width (nm)	Aspect Ratio
8 hr	161 ± 13	-47.2 ± 6.6	709	88.6	467 ± 277	31.9 ± 9.26	14.9 ± 8.54
12 hr	160 ± 30	-42.7 ± 6.8	412	51.5	298 ± 115	28.1 ± 4.69	10.8 ± 4.21
16 hr	134 ± 8.6	-39.7 ± 1.9	294	36.8	257 ± 132	26.1 ± 4.01	10.4 ± 5.24
20 hr	126 ± 12	-44.9 ± 2.0	188	23.5	236 ± 90	28.6 ± 4.74	8.30 ± 2.91
24 hr	137 ± 10	-33.1 ± 5.2	270	33.8	215 ± 120	22.8 ± 3.71	9.47 ± 5.30
36 hr	103 ± 31	-45.4 ± 3.7	200	25	211 ± 112	22.1 ± 4.56	9.56 ± 5.18
48 hr	113 ± 9	-41.3 ± 4.8	22	2.76	159 ± 63	19.9 ± 3.42	8.06 ± 3.09

Note: Data represents mean ± standard deviation.

FTIR analysis

FTIR spectroscopy was employed to compare the chemical structure of CNCs extracted at different reaction times (Fig. 4). In plant-derived cellulose, non-cellulosic components such as lignin and hemicellulose are typically present before extraction (Klemm *et al.* 2005; Brinchi *et al.* 2013; Trache *et al.* 2017). Previous studies reported that the ammonium persulfate (APS) oxidation introduced carboxyl groups onto the CNC particle surface during the extraction process (Hu *et al.* 2014; Zhang *et al.* 2016; Liu et al. 2020). All samples exhibited characteristic cellulose absorption bands at ~ 3340 cm^{-1} (— OH stretching) and ~ 2890 cm^{-1} (C — H stretching), consistent with previous reports (Jiang *et al.* 2017; Oun and Rhim 2018; Kassab *et al.* 2020; Madruga *et al.* 2020; Wang *et al.* 2020; Liu et al. 2020; Marwanto *et al.* 2021; Momeni *et al.* 2021; Vilaça *et al.* 2021; Abbasi Moud 2022; Akshaya *et al.* 2022; Asad and Sana 2023; Im *et al.* 2023; Thu *et al.* 2023). Distinct peaks at 1734 cm^{-1} and 1238 cm^{-1} were observed in the 8-CNC's spectrum, corresponding to lignin (Khanjanzadeh and Park 2021) and hemicellulose (El Achaby *et al.* 2018), respectively. These signals were still weakly detectable in the 12-CNC sample but disappeared in spectra collected from samples treated for ≥ 16 h, indicating that non-cellulosic residues were completely removed after 16 h of reaction time.

A peak at ~ 1604 cm^{-1}, assigned to sodium carboxylate (— $COO^{-}NA^{+}$) [15, 16, 39], was present as early as 8 h and increased intensity up to 24 h, suggesting progressive surface functionalization by APS

oxidation. Interestingly, this peak decreased in intensity beyond 24 h, indicating possible stabilization or partial degradation of surface functionalities with prolonged reaction time.

Aside from these changes, no significant shifts or variations were observed in other characteristic cellulose bands (1424 cm^{-1}, 1160 cm^{-1}, 1102 cm^{-1}, 1030 cm^{-1}, and 898 cm^{-1}), suggesting that APS oxidation primarily modifies the CNC surface without altering the underlying cellulose backbone. These results confirm that APS treatment effectively removes non-cellulosic impurities while imparting surface carboxyl groups, offering a sustainable route to functionalized CNCs. Importantly, the introduction of carboxyl groups enhances CNC hydrophilicity and reactivity, which can improve dispersion in aqueous systems and enable their incorporation into biocomposites, coatings, and packaging materials designed for sustainable applications.

CNC mechanical properties

The mechanical properties of hemp-derived CNCs extracted at different APS oxidation times were evaluated using AFM force-distance spectroscopy (FDS). Previous studies have demonstrated the application of FDS for probing CNC mechanics on flat surfaces, (Wagner et al. 2010) our prior work (Heacock et al. 2024) confirmed that FDS yields consistent results for both isolated and agglomerated CNCs, with no significant differences in Young's modulus (E_T) between the two populations (Wagner et al. 2010; Heacock et al. 2024). This finding is critical, as residual lignin and hemicellulose were observed in early-stage CNCs (Fig. 4) yet were shown not to influence E_T. For this study, adhesion energy and E_T were determined from 50 individual CNCs per group, regardless of aggregation state. Based on the structural and chemical differences observed among samples, detailed mechanical testing was focused on 8-CNC, 24-CNC, and 48-CNC.

Adhesion energies of 198 ± 145 aJ, 170 ± 118 aJ, and 256 ± 215 aJ were measured for 8-CNC, 24-CNC, and 48-CNC, respectively (Fig. 5a and Table 2). Although the 48-CNC sample exhibited a slightly higher mean value, statistical analysis confirmed no significant differences among the groups. These results suggest that APS reaction time does not substantially alter the surface adhesive interaction of CNCs, though further testing may be required to confirm subtle variations.

Young's modulus (E_T) values are presented in Fig. 5b and Table 2. For comparison, Wagner et al. reported E_T values of 2–37 GPa for tunicate-derived CNCs obtained via acid hydrolysis, while the axial elastic modulus (E_A) of wood and tunicate CNCs is generally reported in 110–200 GPa (Wagner et al. 2010). Using APS oxidation, our previous work (Heacock et al. 2024) reported E_T values of ~ 2 GPa for hemp CNCs when measured with CONTSC cantilever (0.2 N/m). In the present study, an NC-LC cantilever (100 N/m) was selected to increase measurements of stiffness and ensure consistency across all samples. The resulting E_T values were 73.3 ± 7.69 GPa (8-CNC), 72.0 ± 6.58 GPa (24-CNC), and 73.5 ± 7.63 GPa (48-CNC). These values fall between those reported for tunicate-derived CNCs by Wagner et al. and the higher axial values cited in the literature (Wagner et al. 2010). Importantly, statistical analysis

revealed no significant differences across reaction times, indicating that APS oxidation duration does not influence the intrinsic stiffness of hemp-derived CNCs.

In summary, these results confirm that APS oxidation provides CNCs with consistent mechanical properties across a broad range of reaction times. This robustness is advantageous for sustainable nanomaterial production, as it suggests flexibility in processing conditions without compromising material performance. Such mechanical stability broadens the potential of APS-derived CNCs for incorporation into biocomposites, coatings, and structural applications in green and circular material systems.

Table 2
Mechanical properties of hemp-derived CNCs at different APS reaction times

Reaction Time (h)	Young's Modulus (GPa)	Adhesion Energy (aJ)
8	73.3 ± 7.69	198 ± 145
24	72.0 ± 6.58	170 ± 118
48	73.5 ± 7.63	256 ± 215

Surface wettability

The wettability of CNC-coated titanium (Ti) surfaces was evaluated using static water contact angle (CA) measurements. The CA, defined as the angle formed at the edge of a water droplet in contact with a solid surface, is a standard indicator of surface hydrophilicity (Zhao and Jiang 2018). Titanium is widely used for biomedical implants due to its biocompatibility, which is strongly influenced by surface properties such as hydrophilicity (Jung *et al.* 2022). Using Ti as a substrate, we investigated how CNC coatings derived at different reaction times influenced surface wettability.

Distinct surface morphologies of Ti substrates were observed across the samples (Fig. 6a-h). Notably, 8-CNC formed a discontinuous film that partially peeled away from the Ti substrate, producing a unique **Fig. 6** Titanium substrates coated with CNCs obtained at different APS reaction times (row 1 and 2) and corresponding surface wettability (i) for 8-CNC (a), 12-CNC (b), 16-CNC (c), 20-CNC (d), 24-CNC (e), 36-CNC (f), 48-CNC (g), and pure Ti (h). *, *** denote $p < 0.05$ and 0.0001, respectively

texture compared to all other samples. In contrast, CNCs prepared at ≥ 12 h adhered more uniformly to the substrate. Several samples (16-CNC, 20-CNC, 24-CNC, and 48-CNC) exhibited a rainbow-like iridescence (Fig. 6c-g), an optical effect attributed to the chiral nematic organization of CNCs (Castro-Guerrero and Gray 2014). Although this optical phenomenon was not directly investigated here, it may provide additional functionality for optical or photonic applications (Wang *et al.* 2020).

Contact angle results are summarized in Fig. 6i. Pure Ti displayed a CA of 73.8°, consistent with its inherently hydrophilic nature (CA < 90°) (Zhao and Jiang 2018). All CNC-coated samples exhibited significantly lower CAs compared to bare Ti, confirming that CNC deposition greatly enhanced surface

hydrophilicity. The 8-CNC sample showed the lowest mean CA (12.8°), although values were widely distributed due to the rapid spreading of water droplets across the irregular film. The extremely high wettability of 8-CNC may be linked to residual hemicellulose, known for its hydrophilic character [45], as suggested by the FTIR results (Fig. 4). Similarly, 12-CNC exhibited a relatively low mean CA of 28.2°, consistent with the partial presence of hemicellulose. By 20 h, the CA increased to 38.9°, the most stable distribution among all samples, suggesting that hemicellulose was fully removed at this stage. Beyond 20 h, CA values decreased again, implying that CNC particle size and surface chemistry may play increasingly important roles in determining hydrophilicity once non-cellulosic residues are eliminated.

Statistical analysis confirmed significant differences in CA among all samples, highlighting that APS reaction time directly influences CNC surface wettability. These results demonstrate that CNC functionalization can be tuned to modify surface interactions, a feature with potential applications in biomedical coatings, sustainable packaging, and other areas where controlled hydrophilicity is essential.

Figure 6i presents a violin plot of the CA measured on the Ti surfaces. This representation was selected to better illustrate the distribution and temporal behavior of CA measurements. A pristine Ti sample (Fig. 6h) was first analyzed as a control. Across all time points, the CA remained below 90°, suggesting the inherent hydrophilic nature of Ti (Zhao and Jiang 2018), with a mean CA value of 73.8°. In contrast, all treated surfaces exhibited significantly lower CA values compared to pristine Ti, implying that CNC coatings enhance surface hydrophilicity of Ti. Among the treated samples, 8-CNC exhibited the lowest mean CA (12.8°). However, the distribution of measured angles was notably broad. This variability is attributed to the rapid spreading of the water droplet immediately upon contact with the surface. Previous work by Zhang et al. reported the intrinsically hydrophilic nature of hemicellulose (Zhang et al. 2011), which may contribute to this behavior. In addition, the pronounced surface topography of 8-CNC (distinct from that of the other samples) along with partial film delamination from the Ti substrate, may further influence the observed wettability. When considered alongside the FTIR results (Fig. 4) and the extremely low CA values observed for 8-CNC (Fig. 6a), these findings suggest that residual hemicellulose remains present and contributes to enhanced hydrophilicity.

This interpretation is further supported by the 12-CNC sample, which exhibited a higher mean CA of 28.2° (Fig. 6i) while still showing evidence of hemicellulose in the FTIR spectra (Fig. 4). In contrast, 20-CNC displayed the most stable CA distribution and the highest mean CA of 38.9° among the treated samples (Fig. 6i), suggesting that hemicellulose had been effectively removed at this reaction time. For reaction time exceeding 20 hours, the CA decreased again, indicating that factors other than hemicellulose, such as CNC particle size, may increasingly influence surface wettability. Additional studies are required to directly assess the role of CNC particle size in governing the hydrophilic behavior of Ti surfaces. Statistical analysis comparing all samples revealed significant differences between each group, demonstrating that surface wettability can be systematically tuned by adjusting APS reaction time.

CNC cytotoxicity

For this study, CNCs at a concentration of 1 mg/mL were suspended in MEM growth medium and incubated with adipose-derived stem cells (ADSCs) for 24 hours. Cytotoxicity was evaluated using a lactate dehydrogenase (LDH) assay, which quantifies cell membrane damage by measuring LDH released into the surrounding medium following cell lysis. A control group consisting of ADSCs cultured in MEM alone was used to represent spontaneous LDH release under normal growth conditions. In addition, a positive cytotoxicity control was prepared by adding Triton X-100 to the culture medium to induce complete membrane lysis and maximal LDH release (Madruga *et al.* 2020; White 2024), following the CyQUANT™ LDH Cytotoxicity Assay Kit protocol. Figure 7 summarizes the LDH release measured for both control groups and all seven CNC samples (8-CNC, 12-CNC, 16-CNC, 20-CNC, 24-CNC, 36-CNC, and 48-CNC). All CNC-treated samples exhibited substantially lower LDH release compared to the Triton-treated group and showed no statistically significant difference relative to the control group. These results indicate that none of the CNC samples exhibited cytotoxic effects toward ADSCs under the tested conditions.

It should be noted that this assessment was conducted using CNCs dispersed in culture medium. Further studies involving CNC-coated substrates (e.g., Ti) in direct contact with cells are necessary to fully validate biocompatibility. In addition, hemocompatibility and long-term cell viability studies are recommended to determine whether CNC reaction times influence cellular responses and to support the potential use of these materials in biomedical applications.

Conclusion

This study demonstrates that APS swelling and oxidation reaction time, spanning 8 to 48 h, plays a critical role in governing the physicochemical properties of hemp-derived CNCs during extraction. Variations in surface chemistry, colloidal stability, and particle size were confirmed through FTIR analysis, long-term aqueous suspension observation, and AFM imaging, respectively. Although surface charge was also influenced by reaction time, no clear or systematic trend was observed. Mechanical testing of representative samples (8-CNC, 24-CNC, and 48-CNC) revealed no statistically significant difference in intrinsic mechanical properties, suggesting that reaction time does not adversely affect the mechanical integrity of the CNCs. When applied as coatings on Ti substrates, CNCs extracted at different reaction times produced distinct changes in surface wettability, demonstrating that reaction time can be used as a controllable parameter to tune interfacial properties. In addition, a cytotoxicity assessment confirmed that APS-oxidized CNCs are non-cytotoxic, with no observed dependence on reaction time under the condition studied. Collectively, these results suggest that reaction time provides a practical means to precisely tailor CNC properties for targeted applications, particularly in the context of biomedical and implantable materials. Future work should focus on improving the stability and durability of CNC attachment to Ti surfaces, as well as conducting comprehensive hemocompatibility and cell viability studies to evaluate further the suitability of these materials for use in Ti-based implants and other biomedical applications.

Declarations

Declaration of competing interest

The authors declare that they have no known competing financial interests or personal relationships that could have appeared to influence the work reported in this paper.

Credit author contribution statement

Jesse A. Heacock: Conceptualization, Methodology, Investigation, Formal Analysis, Writing – original draft.

Mahboube Piryaee: Investigation, data curation, Writing – Editing.

Morgan Davis: Data collection and analysis.

Yan Vivian Li: Supervision, Conceptualization, Methodology, Writing – Review & Editing, Funding acquisition.

Funding:

The Colorado Agricultural Experimental Station Grant (COL00408) and the Advanced Industries Accelerator Grant (CTGG1 2024–2087) by the Colorado Office of Economic Development & International Trade.

Acknowledgment: This work was supported by the Colorado Agricultural Experimental Station Grant (COL00408) and the Advanced Industries Accelerator Grant (CTGG1 2024–2087) by the Colorado Office of Economic Development & International Trade. The authors would like to acknowledge the ARC Materials and Molecular Analysis (MMA) at Colorado State University for providing equipment for material characterizations.

Author Contribution

Jesse A. Heacock: Conceptualization, Methodology, Investigation, Formal Analysis, Writing – original draft.Mahboube Piryaee: Investigation, data curation, Writing – Editing.Morgan Davis: Data collection and analysis.Liming Zou: Conceptualization, Methodology - Review & Editing.Yan Vivian Li: Supervision, Conceptualization, Methodology, Writing – Review & Editing, Funding acquisition.

Acknowledgement

This work was supported by the Colorado Agricultural Experimental Station Grant (COL00408) and the Advanced Industries Accelerator Grant (CTGG1 2024-2087) by the Colorado Office of Economic Development & International Trade. The authors would like to acknowledge the ARC Materials and Molecular Analysis (MMA) at Colorado State University for providing equipment for material characterizations.

Data availability

The data that support the findings of this study are available from the corresponding author upon reasonable request.

References

1. Abbasi Moud A (2022) Cellulose nanocrystals examined by atomic force microscopy: applications and fundamentals. ACS Food Sci Technol 2:1789–1818. https://doi.org/10.1021/acsfoodscitech.2c00289
2. Akshaya S, Rowlo PK, Dukle A, Nathanael AJ (2022) Antibacterial coatings for titanium implants: recent trends and future perspectives. Antibiotics 11:1719. https://doi.org/10.3390/antibiotics11121719
3. Asad M, Sana M (2023) Potential of titanium based alloys in the biomedical sector and their surface modification techniques: a review. Proc Inst Mech Eng C J Mech Eng Sci 237:5503–5532. https://doi.org/10.1177/09544062231164506
4. Bashar MM, Zhu H, Yamamoto S, Mitsuishi M (2019) Highly carboxylated and crystalline cellulose nanocrystals from jute fiber by facile ammonium persulfate oxidation. Cellulose 26:3671–3684. https://doi.org/10.1007/s10570-019-02363-7
5. Benhamou K, Dufresne A, Magnin A, Mortha G, Kaddami H (2014) Control of size and viscoelastic properties of nanofibrillated cellulose from palm tree by varying the TEMPO-mediated oxidation time. Carbohydr Polym 99:74–83. https://doi.org/10.1016/j.carbpol.2013.08.032
6. Brinchi L, Cotana F, Fortunati E, Kenny JM (2013) Production of nanocrystalline cellulose from lignocellulosic biomass: technology and applications. Carbohydr Polym 94:154–169. https://doi.org/10.1016/j.carbpol.2013.01.033
7. Castro-Guerrero CF, Gray DG (2014) Chiral nematic phase formation by aqueous suspensions of cellulose nanocrystals prepared by oxidation with ammonium persulfate. Cellulose 21:2567–2577. https://doi.org/10.1007/s10570-014-0308-1
8. Culsum NTU, Melinda C, Leman I, Wibowo A, Budhi YW (2021) Isolation and characterization of cellulose nanocrystals (CNCs) from industrial denim waste using ammonium persulfate. Mater Today Commun 26:101817. https://doi.org/10.1016/j.mtcomm.2020.101817
9. Delepierre G, Vanderfleet OM, Niinivaara E, Zakani B, Cranston ED (2021) Benchmarking cellulose nanocrystals Part II: new industrially produced materials. Langmuir 37:8393–8409.

https://doi.org/10.1021/acs.langmuir.1c00550

10. El Achaby M, Kassab Z, Barakat A, Aboulkas A (2018) Alfa fibers as viable sustainable source for cellulose nanocrystals extraction: application for improving the tensile properties of biopolymer nanocomposite films. Ind Crops Prod 112:499–510. https://doi.org/10.1016/j.indcrop.2017.12.049
11. Filipova I, Serra F, Tarres Q, Mutje P, Delgado-Aguilar M (2020) Oxidative treatments for cellulose nanofibers production: a comparative study between TEMPO-mediated and ammonium persulfate oxidation. Cellulose 27:10671–10688. https://doi.org/10.1007/s10570-020-03089-7
12. Haunreiter KJ, Dichiara AB, Gustafson R (2022) Nanocellulose by ammonium persulfate oxidation: an alternative to TEMPO-mediated oxidation. ACS Sustain Chem Eng 10:3882–3891. https://doi.org/10.1021/acssuschemeng.1c07814
13. Heacock JA, Sun Y, Li YV (2024) Mechanical and morphological properties of cellulose nanocrystals extracted from industrial hemp agro-waste. Cellulose 31:10861–10877. https://doi.org/10.1007/s10570-024-06255-3
14. Hu Y, Tang L, Lu Q, Wang S, Chen X, Huang B (2014) Preparation of cellulose nanocrystals and carboxylated cellulose nanocrystals from borer powder of bamboo. Cellulose 21:1611–1618. https://doi.org/10.1007/s10570-014-0236-0
15. Im JS, Choi H, An HW, Kwon TY, Hong MH (2023) Effects of surface treatment method forming new nano/micro hierarchical structures on attachment and proliferation of osteoblast-like cells. Materials 16:5717. https://doi.org/10.20944/preprints202307.0665.v1
16. Jiang H, Wu Y, Han B, Zhang Y (2017) Effect of oxidation time on the properties of cellulose nanocrystals from hybrid poplar residues using the ammonium persulfate. Carbohydr Polym 174:291–298. https://doi.org/10.1016/j.carbpol.2017.06.080
17. Jiang P, Zhang Y, Hu R, Shi B, Zhang L, Huang Q, et al (2023) Advanced surface engineering of titanium materials for biomedical applications: from static modification to dynamic responsive regulation. Bioact Mater 27:15–57. https://doi.org/10.1016/j.bioactmat.2023.03.006
18. Jung J, Choi YJ, Lee SJ, Choi YS, Douangdeuane B, Souliya O, et al (2022) Promoting effects of titanium implants coated with Dipterocarpus tuberculatus extract on osseointegration. ACS Biomater Sci Eng 8:847–858. https://doi.org/10.1021/acsbiomaterials.1c01220
19. Kang X, Kuga S, Wang C, Zhao Y, Wu M, Huang Y (2018) Green preparation of cellulose nanocrystal and its application. ACS Sustain Chem Eng 6:2954–2960. https://doi.org/10.1021/acssuschemeng.7b02363
20. Kassab Z, Abdellaoui Y, Salim MH, Bouhfid R, Qaiss AEK, El Achaby M (2020) Micro- and nano-celluloses derived from hemp stalks and their effect as polymer reinforcing materials. Carbohydr Polym 245:116506. https://doi.org/10.1016/j.carbpol.2020.116506
21. Khanjanzadeh H, Park BD (2021) Optimum oxidation for direct and efficient extraction of carboxylated cellulose nanocrystals from recycled MDF fibers by ammonium persulfate. Carbohydr Polym 251:117029. https://doi.org/10.1016/j.carbpol.2020.117029

22. Klemm D, Heublein B, Fink HP, Bohn A (2005) Cellulose: fascinating biopolymer and sustainable raw material. Angew Chem Int Ed 44:3358–3393. https://doi.org/10.1002/anie.200460587
23. Lam E, Leung AC, Liu Y, Majid E, Hrapovic S, Male KB, Luong JH (2013) Green strategy guided by Raman spectroscopy for the synthesis of ammonium carboxylated nanocrystalline cellulose and the recovery of byproducts. ACS Sustain Chem Eng 1:278–283. https://doi.org/10.1021/sc3001367
24. Leung AC, Hrapovic S, Lam E, Liu Y, Male KB, Mahmoud KA, Luong JH (2011) Characteristics and properties of carboxylated cellulose nanocrystals prepared from a novel one-step procedure. Small 7:302–305. https://doi.org/10.1002/smll.201001715
25. Liu Y, Liu L, Wang K, Zhang H, Yuan Y, Wei H, et al (2020) Modified ammonium persulfate oxidations for efficient preparation of carboxylated cellulose nanocrystals. Carbohydr Polym 229:115572. https://doi.org/10.1016/j.carbpol.2019.115572
26. Liu Y, Rath B, Tingart M, Eschweiler J (2020) Role of implants surface modification in osseointegration: a systematic review. J Biomed Mater Res A 108:470–484. https://doi.org/10.1002/jbm.a.36829
27. Madani H, Wibowo A, Judawisastra H, Nishiyama N, Budhi YW (2022) One-step extraction of cellulose nanocrystals from high lignin biomass through ammonium persulfate oxidation method. Adv Nat Sci Nanosci Nanotechnol 13:015007. https://doi.org/10.1088/2043-6262/ac549a
28. Madruga LY, Sabino RM, Santos EC, Popat KC, Balaban RDC, Kipper MJ (2020) Carboxymethyl-kappa-carrageenan: a study of biocompatibility, antioxidant and antibacterial activities. Int J Biol Macromol 152:483–491. https://doi.org/10.1016/j.ijbiomac.2020.02.274
29. Mali P, Sherje AP (2022) Cellulose nanocrystals: fundamentals and biomedical applications. Carbohydr Polym 275:118668. https://doi.org/10.1016/j.carbpol.2021.118668
30. Man Z, Muhammad N, Sarwono A, Bustam MA, Vignesh Kumar M, Rafiq S (2011) Preparation of cellulose nanocrystals using an ionic liquid. J Polym Environ 19:726–731. https://doi.org/10.1007/s10924-011-0323-3
31. Marwanto M, Maulana MI, Febrianto F, Wistara NJ, Nikmatin S, Masruchin N, et al (2021) Effect of oxidation time on the properties of cellulose nanocrystals prepared from balsa and kapok fibers using ammonium persulfate. Polymers 13:1894. https://doi.org/10.3390/polym13111894
32. Momeni S, Safder M, Khondoker MAH, Elias AL (2021) Valorization of hemp hurds as bio-sourced additives in PLA-based biocomposites. Polymers 13:3786. https://doi.org/10.3390/polym13213786
33. Novo LP, Bras J, García A, Belgacem N, Curvelo AA (2015) Subcritical water: a method for green production of cellulose nanocrystals. ACS Sustain Chem Eng 3:2839–2846. https://doi.org/10.1021/acssuschemeng.5b00762
34. Oun AA, Rhim JW (2018) Isolation of oxidized nanocellulose from rice straw using the ammonium persulfate method. Cellulose 25:2143–2149. https://doi.org/10.1007/s10570-018-1730-6
35. Patil TV, Patel DK, Dutta SD, Ganguly K, Santra TS, Lim KT (2022) Nanocellulose, a versatile platform: from the delivery of active molecules to tissue engineering applications. Bioact Mater 9:566–589. https://doi.org/10.1016/j.bioactmat.2021.07.006

36. Piryaee M, Karder HG, Khodaei M (2025) Hydrophobic anodized alumina surface with embedded CuO nanoparticles: a study on antibacterial behavior. Open Ceram 22:100786. https://doi.org/10.1016/j.oceram.2025.100786
37. Punia Bangar S, Ilyas RA, Chaudhary N, Dhull SB, Chowdhury A, Lorenzo JM (2023) Plant-based natural fibers for food packaging: a green approach to the reinforcement of biopolymers. J Polym Environ 31:5029–5049. https://doi.org/10.1007/s10924-023-02849-3
38. Thu MK, Kang YS, Kwak JM, Jo YH, Han JS, Yeo ISL (2023) Comparison between bone-implant interfaces of microtopographically modified zirconia and titanium implants. Sci Rep 13:11142. https://doi.org/10.1038/s41598-023-38432-y
39. Trache D, Hussin MH, Haafiz MM, Thakur VK (2017) Recent progress in cellulose nanocrystals: sources and production. Nanoscale 9:1763–1786. https://doi.org/10.1039/C6NR09494E
40. Vilaça A, Domingues RM, Tiainen H, Mendes BB, Barrantes A, Reis RL, et al (2021) Multifunctional surfaces for improving soft tissue integration. Adv Healthc Mater 10:2001985. https://doi.org/10.1002/adhm.202001985
41. Wagner R, Raman A, Moon R (2010) Transverse elasticity of cellulose nanocrystals via atomic force microscopy. Cellulose 7:27.
42. Wang H, Pudukudy M, Ni Y, Zhi Y, Zhang H, Wang Z, et al (2020) Synthesis of nanocrystalline cellulose via ammonium persulfate-assisted swelling followed by oxidation and their chiral self-assembly. Cellulose 27:657–676. https://doi.org/10.1007/s10570-019-02789-z
43. White A (2024) LDH cytotoxicity assay.
44. Zhang K, Sun P, Liu H, Shang S, Song J, Wang D (2016) Extraction and comparison of carboxylated cellulose nanocrystals from bleached sugarcane bagasse pulp using two different oxidation methods. Carbohydr Polym 138:237–243. https://doi.org/10.1016/j.carbpol.2015.11.038
45. Zhang Y, Hosseinaei O, Wang S, Zhou Z (2011) Influence of hemicellulose extraction on water uptake behavior of wood strands. Wood Fiber Sci 244–250.
46. Zhao T, Jiang L (2018) Contact angle measurement of natural materials. Colloids Surf B Biointerfaces 161:324–330. https://doi.org/10.1016/j.colsurfb.2017.10.056

Figures

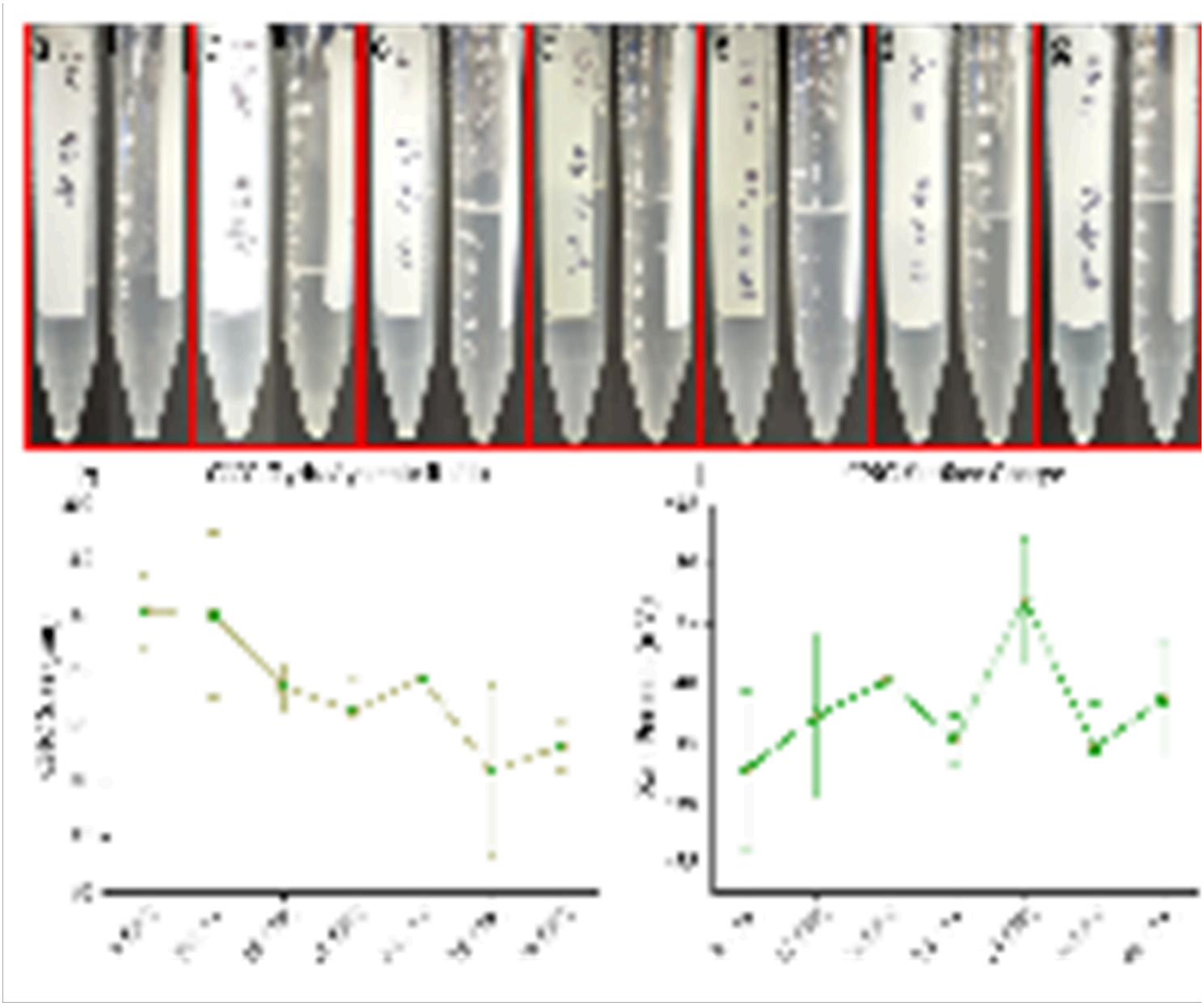


Figure 1

4% w/v CNC aqueous dispersions (top row), DLS hydrodynamic radius (h), and Zeta potential (i) of 8-CNC (a), 12-CNC (b), 16-CNC (c), 20-CNC (d), 24-CNC (e), 36-CNC (f), and 48-CNC (g).

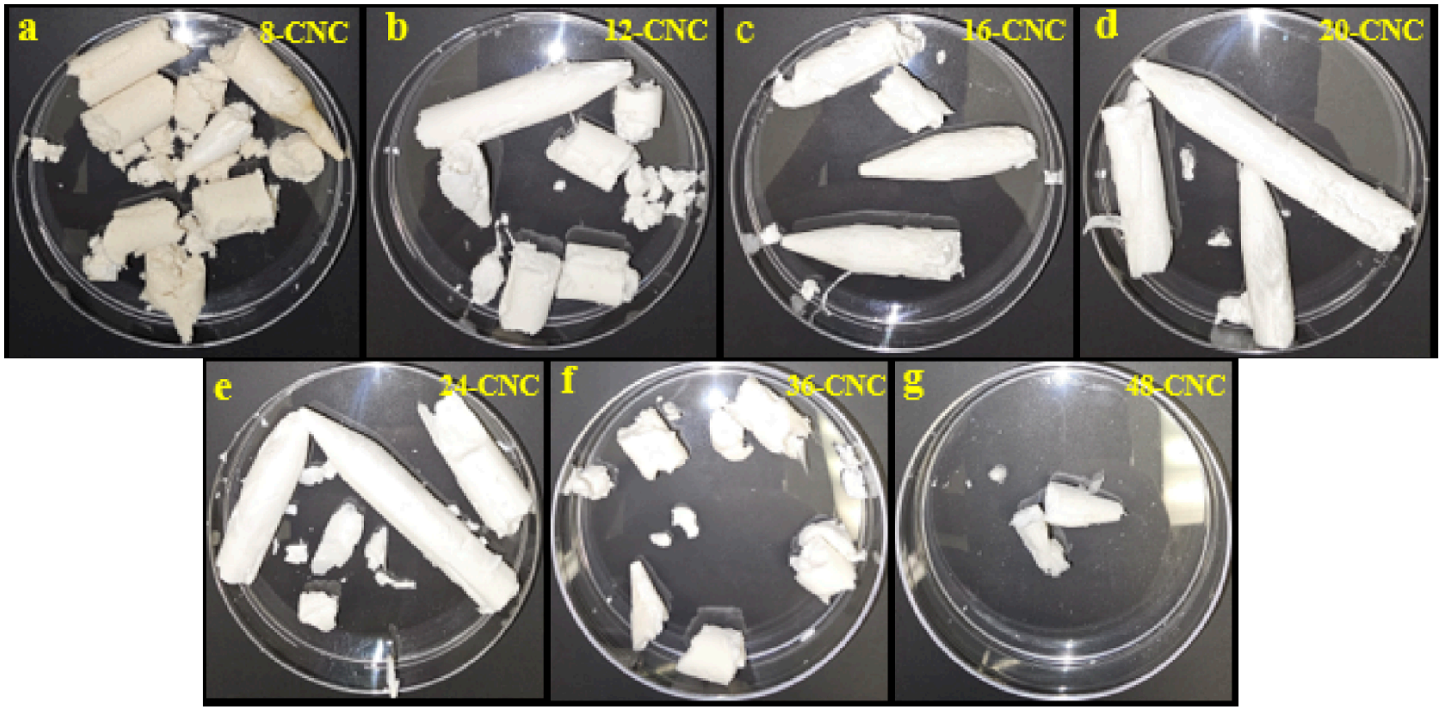


Figure 2

Dried CNC samples: 8-CNC (a), 12-CNC (b), 16-CNC (c), 20-CNC (d), 24-CNC (e), 36-CNC (f), and 48-CNC (g).

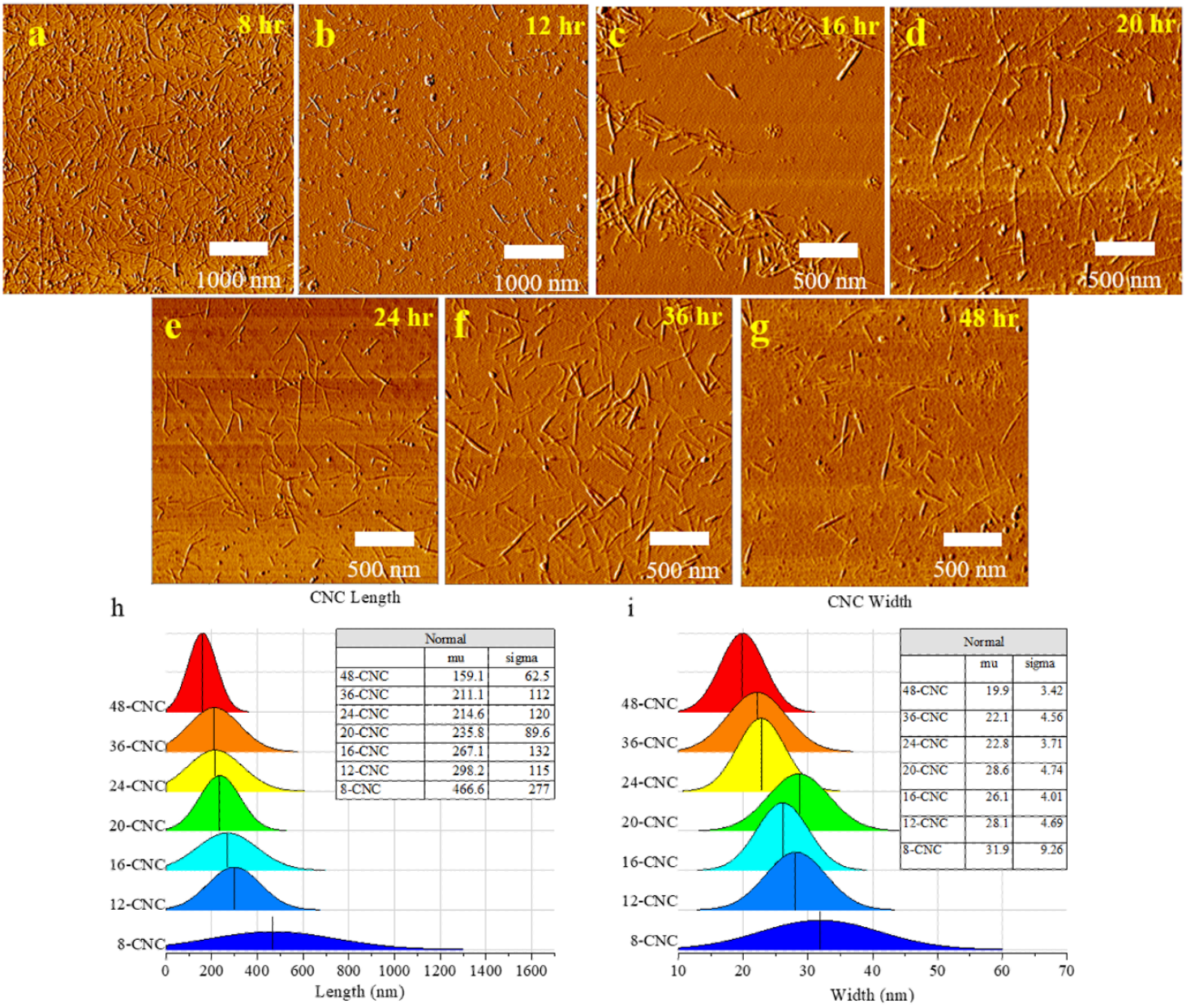


Figure 3

AFM images (first and second rows), length distribution (h), and width distribution (i) of 8-CNC (a), 12-CNC (b), 16-CNC (c), 20-CNC (d), 24-CNC (e), 36-CNC (f), and 48-CNC (g).

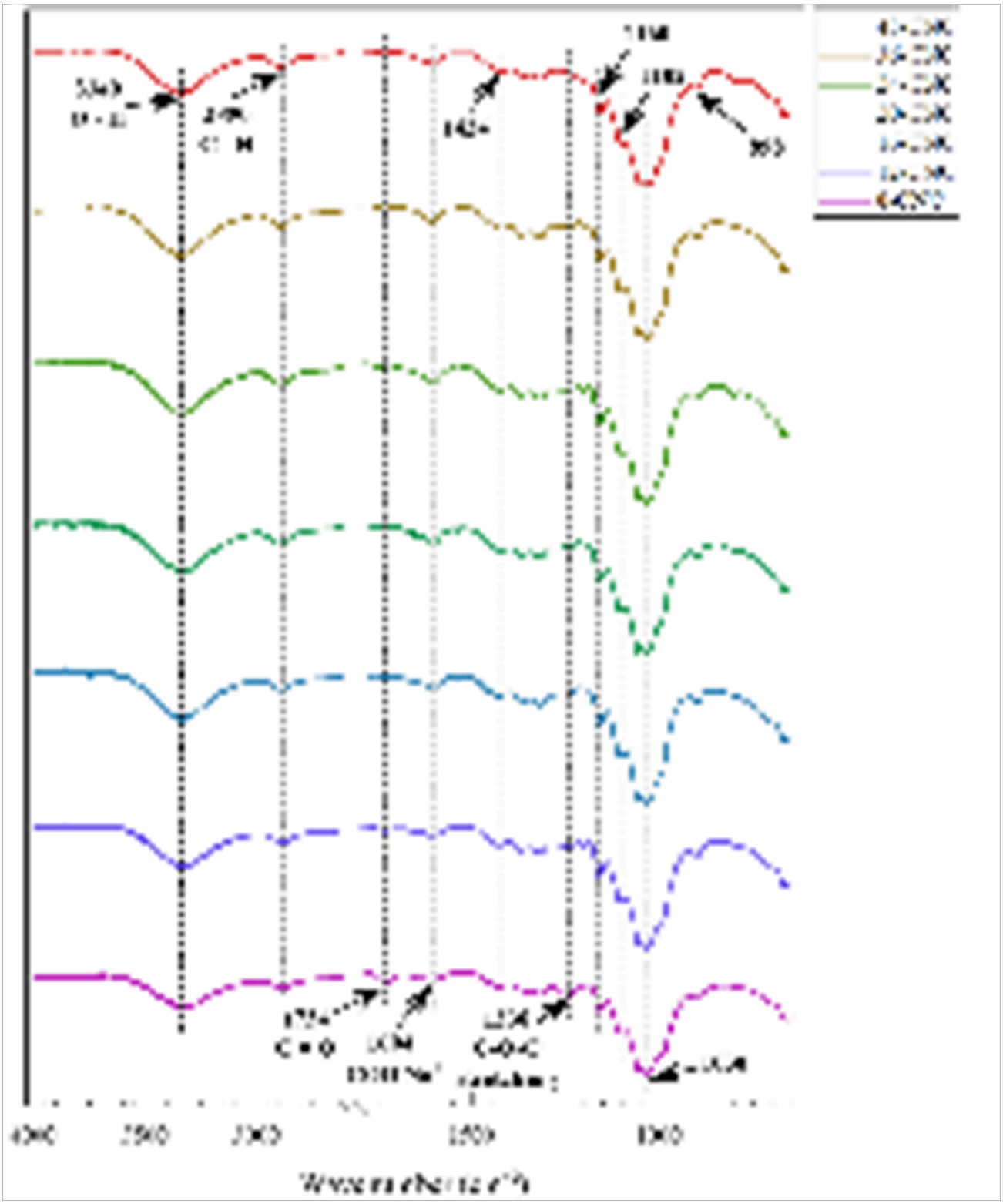


Figure 4

FTIR spectra of hemp-derived CNCs extracted at different reaction times (8, 12, 16, 20, 24, 36, and 48 h).

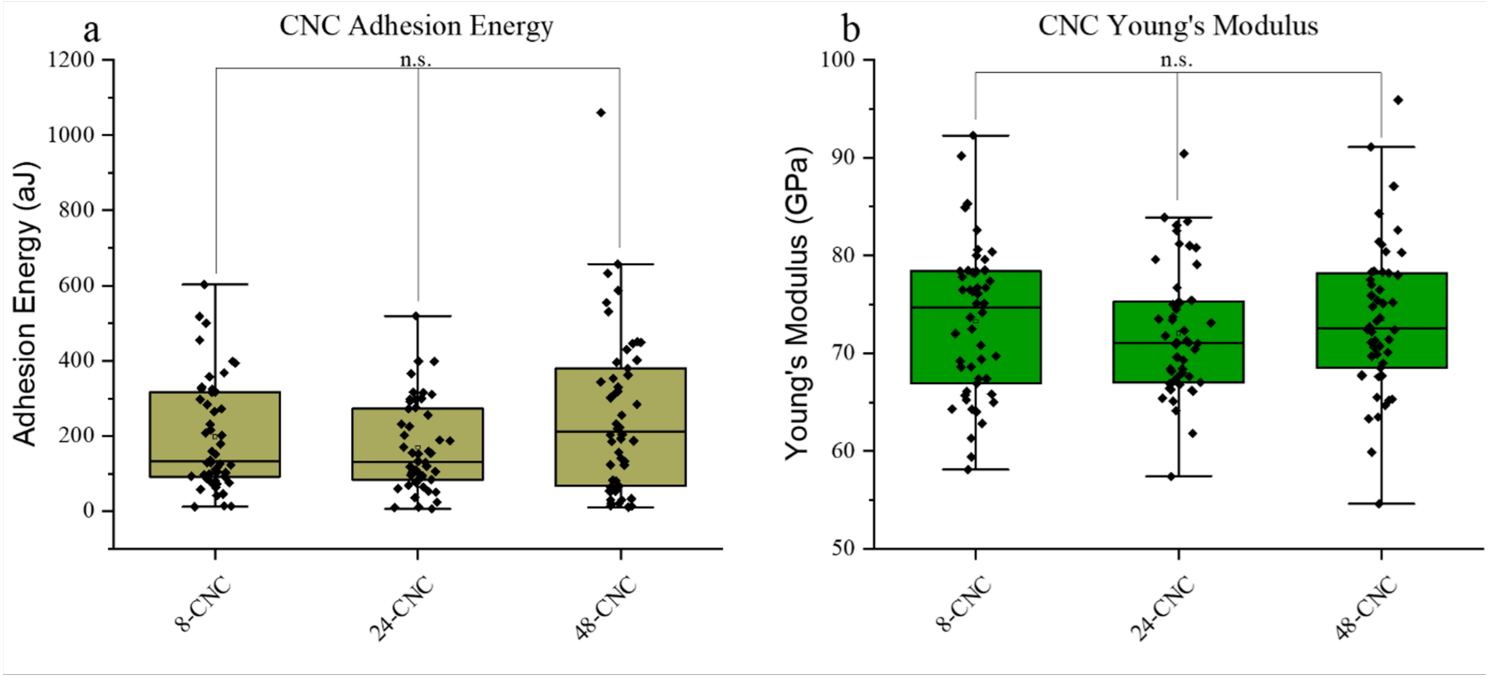


Figure 5

AFM-FDS adhesion energy (a) and Young's modulus (b) of 8CNC, 24-CNC, and 48-CNC.

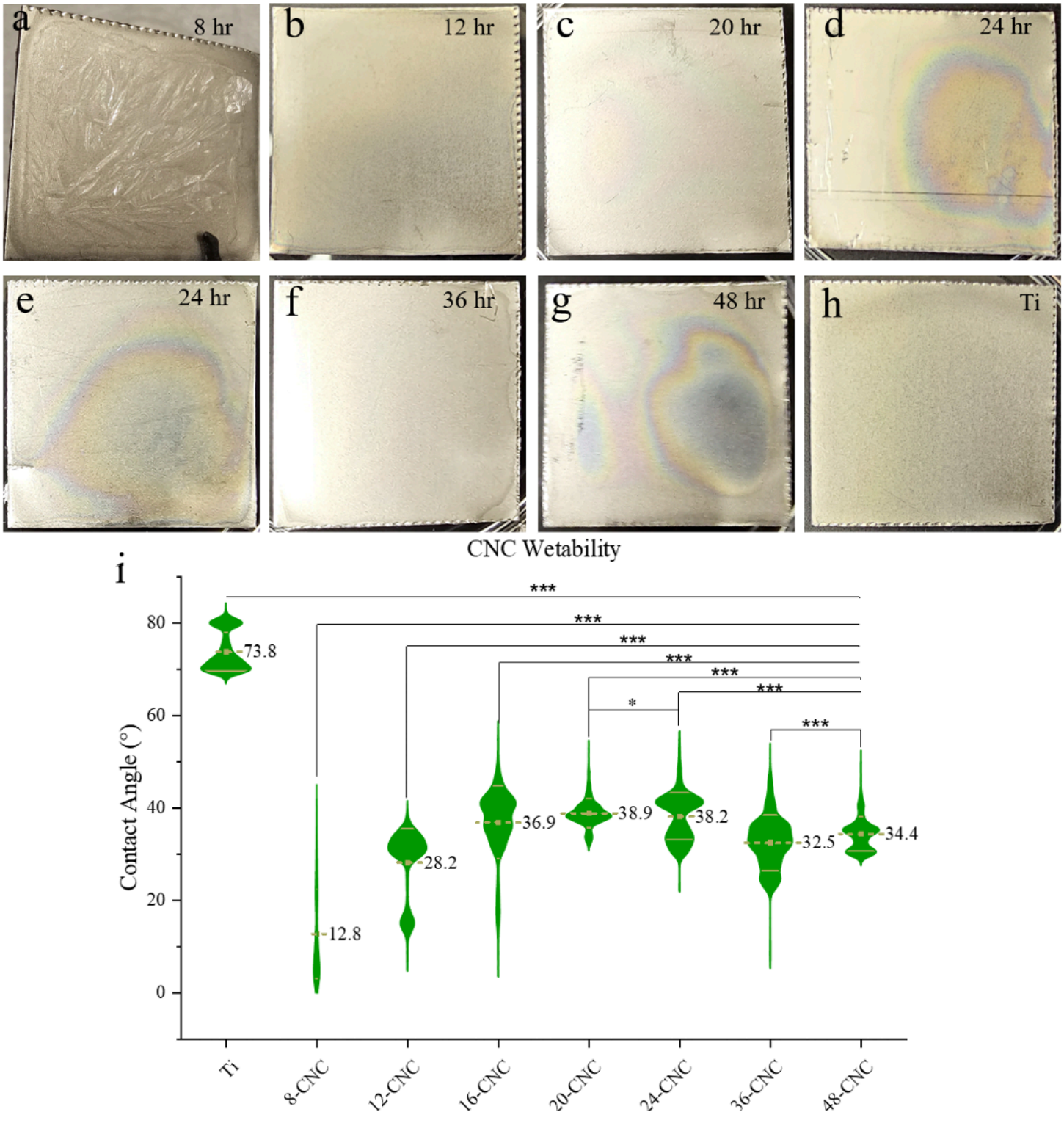


Figure 6

Titanium substrates coated with CNCs obtained at different APS reaction times (row 1 and 2) and corresponding surface wettability (i) for 8-CNC (a), 12-CNC (b), 16-CNC (c), 20-CNC (d), 24-CNC (e), 36-CNC (f), 48-CNC (g), and pure Ti (h). *, *** denote $p < 0.05$ and 0.0001, respectively.

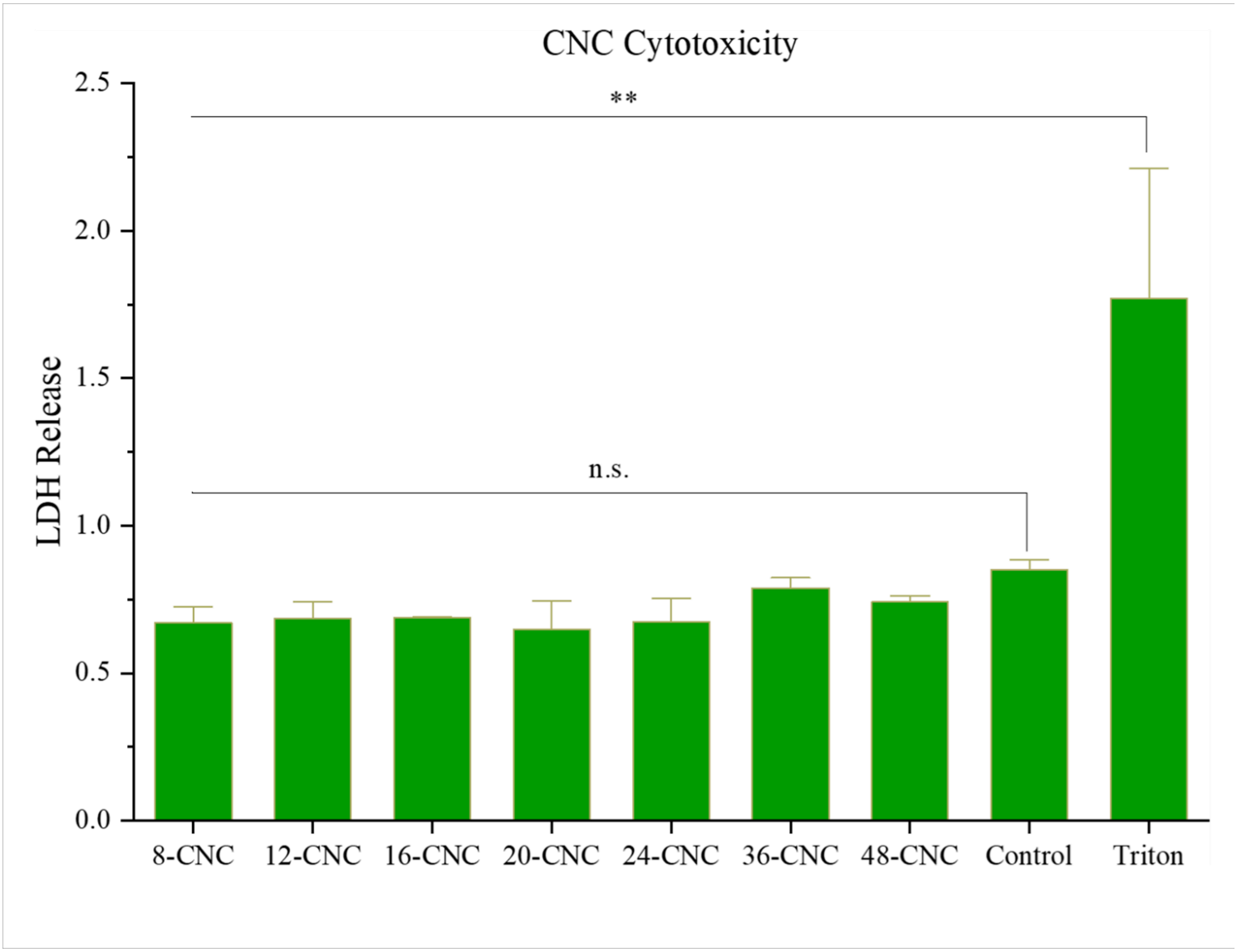


Figure 7

Cytotoxicity studies of CNCs against ADSCs. The values are represented as absorbance values at 490 and 680 nm. Control and Triton represent spontaneous and maximum LDH release values. Statistical significance was assessed by one-way ANOVA. ** indicates $p < 0.01$ and n.s. indicates no significant difference.

Supplementary Files

This is a list of supplementary files associated with this preprint. Click to download.

- Tables.docx
- Graphicabstract.tif